Photophysical and Magnetic Properties in Complexes Containing 3d/4f Elements and Chiral Phenanthroline-Based Helicate-Like Ligands

Saskia Speed, Fabrice Pointillart, Jean-Christophe Mulatier, Laure Guy, Stéphane Golhen, Olivier Cador, Boris Le Guennic, François Riobé, Olivier Maury, Lahcène Ouahab

Photophysical and Magnetic Properties in Complexes Associating 3d/4f Elements and Chiral Phenantroline-based Helicate Like Ligands

Saskia Speed,[a] Fabrice Pointillart,*[a] Jean-Christophe Mulatier,[b] Laure Guy,*[b] Stéphane Golhen,[a] Olivier Cador,[a] Boris Le Guennic,[a] François Riobé,[b] Olivier Maury,[b] Lahcène Ouahab[a]

Keywords: Helicene / Lanthanides / Iron/ Chirality / Luminescence / Magnetic properties

The reaction between the chiral helicene-like ligand (**L**) and either $Ln(hfac)_3{\cdot}2H_2O$ ($hfac^-$ = 1,1,1,5,5,5-hexafluoroacetylacetonate), $Ln(tta)_3{\cdot}2H_2O$ (tta^- = 2-tenoyltrifluoroacetonate), a sulfate or chloride Fe^{II} salt, or a combination of them led to the formation of five chiral 4*f* compounds of formula [**HL**][Ln(hfac)$_4$]·n CH_2Cl_2 (Ln = Dy, n = 0.5 (**1**) and Ln = Yb, n = 1 (**2**)), [**HL**][Ln(tta)$_4$]·nC_6H_{14} (Ln = Dy, n = 0 (**3**) and Ln = Yb, n = 2.5 (**4**)) and [**HL**]$_2$[Yb_8(hfac)$_{12}$(OH)$_{12}$(O)]·0.5C_6H_{14}·H_2O (**5**), a chiral 3*d* complex of formula [Fe(NCS)$_2$(**L**)]·CH_3NO_2 (**6**) and a chiral 3*d*4*f* heterobimetallic compound of formula [Fe(tta)(**L**)][Dy(tta)$_4$]·2.5CH_2Cl_2 (**7**). The influence of the nature of the ancillary ligand and of the presence/absence of base during the synthesis on the homochirality/heterochirality arrangement of the ligands as well as the dimension and nuclearity of the edifices is studied. Ytterbium-based compounds **2**, **4** and **5** displayed near-infrared luminescence under irradiation at 350 nm due to the $^2F_{5/2} \rightarrow {}^2F_{7/2}$ Yb^{III} transition (centered at 1000 nm). Complex **2** displayed a second NIR emission at 1278 nm that is attributed to singlet oxygen phosphorescence O_2 ($a^1\Delta_g \rightarrow X^3\Sigma_g^-$) at both room temperature and 77 K. Dynamic magnetic measurements showed the appearance of an out-of-phase signal for the magnetic susceptibility of compound **7** which can be depicted as a 3*d*4*f* chiral heterobimetallic single molecule magnet.

[a] Institut des Sciences Chimiques de Rennes, UMR 6226 CNRS-Université de Rennes 1, 263 Avenue du Général Leclerc 35042 Rennes Cedex, France.
Tel : +33223236752
E-mail: fabrice.pointillart@univ-rennes1.fr
http://www.scienceschimiques.univ-rennes1.fr

[b] Univ Lyon, ENS de Lyon, Université Claude Bernard Lyon 1, CNRS UMR 5182, Laboratoire de Chimie, F69342, Lyon, France.

Supporting information for this article is available on the WWW under http://www.eurjic.org/ or from the author.

Introduction

Chemists and physicists are fascinated by coordination complexes that present exciting physical properties such as magnetism, chirality or luminescence. The elaboration of molecular magnets is motivated by the possibility to observe spin crossover[1] and single molecule magnet (SMM) behaviours[2] using transition metals or lanthanides. The observation of memory effect in this kind of compounds makes them promising candidates for several applications such as spintronics, high-density data storage or quantum computing.[3] One of the main actual challenges consists in combining more than one property in a unique molecular system. Until now, the greatest success is probably the synergy between long-range magnetic ordering and chirality leading to the observation of intense magnetochiral effect.[4] More recently, the use of lanthanide ions allowed the emergence of a new class of luminescent SMM[5] which can also be chiral in rare cases.[6] In the latter, the organic ligands carry the chirality function. Nevertheless, their optical activity is quite low and new types of ligands, such as helicene and binaphtalene have to be considered. They present high optical rotation values[7] and uncommon capabilities in enantioselective catalysis,[8] molecular recognition,[9] nonlinear optics[10] and have been also used as precursor for liquid crystals[11] or components for molecular devices;[12] thus not primarily designed for coordination reactions.

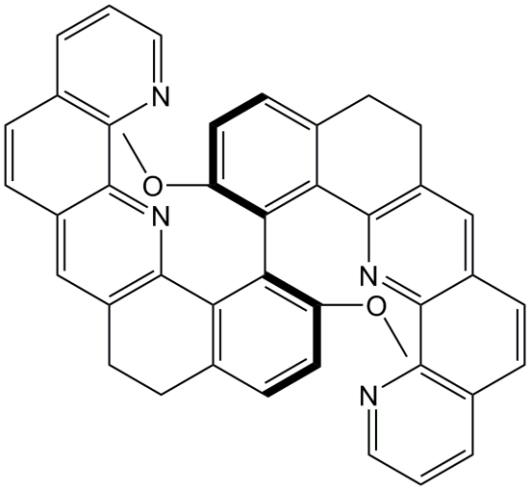

Scheme 1. Chemical structures of **L**.

Few years ago, some of us published the synthesis of dibenzo[*c*]acridine helicene-like ligands involving pyridine moieties that exhibited high chiroptic properties.[13] We modified this ligand by introducing a phenanthroline moieties (**L** = tetrahydro-13,13'-binaphtho[1,2-*b*][1,10]phenanthrolines, scheme 1) able to coordinate either transition metals and lanthanide ions . In this article, we first describe the synthesis of the racemic **L** and **HL** ligands as well as their X-ray structures on single crystals and then explore the reactivity of the ligand **L** in presence of either Ln(β-diketonate)$_3{\cdot}2H_2O$ (β-diketonate = $hfac^-$ (1,1,1,5,5,5-hexafluoroacetyacetonate) and tta^- (2-thenoyltrifluoroacetonate)), sulfate Fe^{II} salt or both Ln^{III} and chloride Fe^{II} salt. Seven X-ray structures of compounds involving **L** or **HL** have been obtained and both their magnetic and optical properties have been studied.

Results and Discussion

Crystal structure analysis

L·2H$_2$O (L). The ligand in its neutral form crystallizes in the Pbcn (N°60) orthorhombic space group (Table 1). The asymmetric unit is composed of one half molecule of **L** and one water molecule of crystallization (Figure 1).

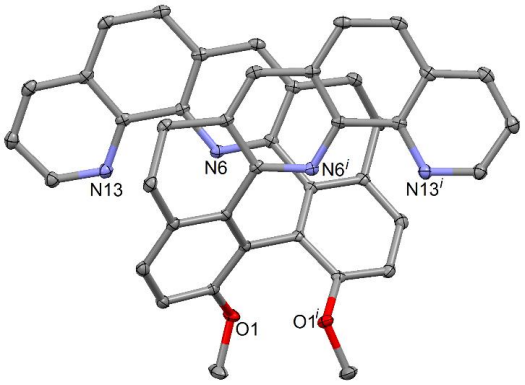

Figure 1. ORTEP view of **L**. Thermal ellipsoids are drawn at 30% probability. Hydrogen atoms and water molecules of crystallization are omitted for clarity. Colour code: grey, carbon atoms; red, oxygen atoms; blue, nitrogen atoms.

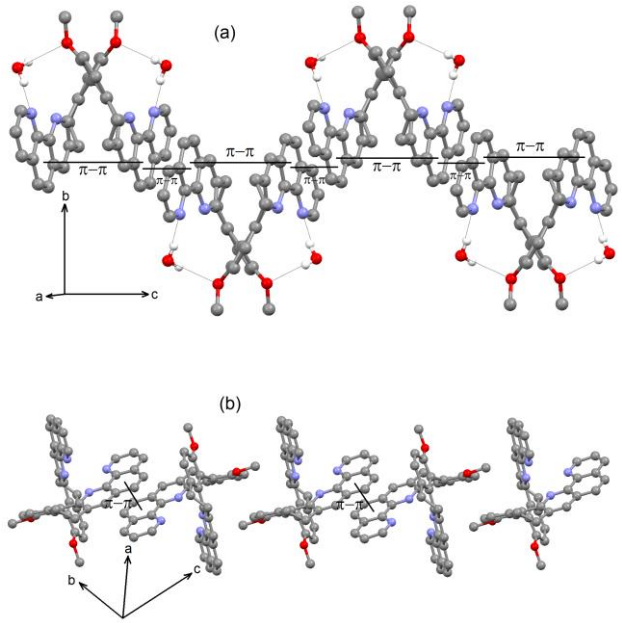

Figure 2. (a) Packing view of **L** highlighting the hydrogen bonds between water molecules and **L**. (b) Packing view of **HL** highlighting the π-π stacking between the aromatic moieties.

The crystal structure shows that the phenantroline moieties are almost parallel in order to induce intramolecular π-π interactions (Figure 1). The water molecules interact with **L** through hydrogen bonds between the methoxy groups and nitrogen atoms of the phenantroline (N13···O25 = 2.808 Å and O1···O25 = 3.024 Å) (Figure 2a). The crystal packing reveals that each molecule of **L** is stacked with the neighbouring molecule through intermolecular π-π interactions between the phenantroline units along the *c* axis (Figure 2b).

(HL)BF$_4$·CH$_2$Cl$_2$ (HL). The ligand in its protonated form crystallizes in the P-1 (N°2) triclinic space group (Table 1). The asymmetric unit is composed by one molecule of protonated **L**, one BF_4^- anion and one dichloromethane molecule of crystallization (Figure 3).

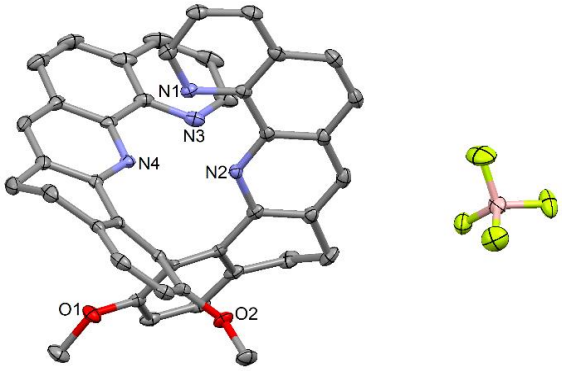

Figure 3. ORTEP view of **HL**. Thermal ellipsoids are drawn at 30% probability. Hydrogen atoms and CH_2Cl_2 molecule of crystallization are omitted for clarity. Colour code: grey, carbon atoms; red, oxygen atoms; blue, nitrogen atoms; pink, boron atom; green, fluoride atoms.

The N2 atom is protonated leading to almost perpendicular arrangement of the two phenantroline moieties in order to form intramolecular hydrogen bonds with the neighbouring nitrogen atoms (N2···N3 = 2.966 Å and N2···N4 = 2.782 Å). The protonation induces drastic changes in the conformation of the molecule that could be interesting for chiroptic properties. The packing shows that the protonated molecules interact through π-π interactions between the phenantroline and benzomethoxy moieties (Figure 2b).

[HL][Ln(hfac)$_4$]·n CH$_2$Cl$_2$(Ln = Dy, n = 0.5 (1) and Ln = Yb, n = 1 (2)). Both complexes are very similar at the molecular scale.

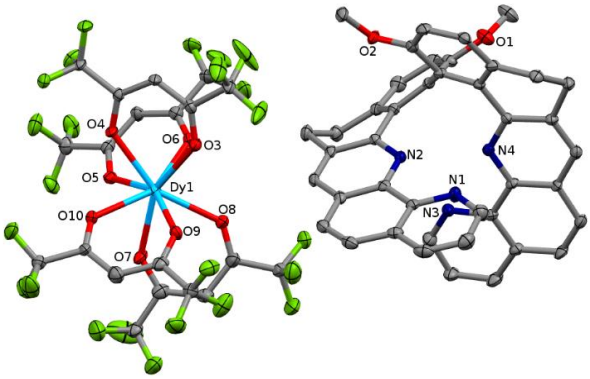

Figure 4. ORTEP view of **1**. Thermal ellipsoids are drawn at 30% probability. Hydrogen atoms and CH_2Cl_2 molecule of crystallization are omitted for clarity. Colour code: grey, carbon atoms; red, oxygen atoms; blue, nitrogen atoms; green, fluoride atoms; light blue, dysprosium atom.

Table 1**.** X-ray crystallographic data for the ligands **L**, (**HL)** and complexes **1**-**7**.

Compounds	**(L)**·2H$_2$O	**[HL]**[Dy(hfac)$_4$]·0.5CH$_2$Cl$_2$ **(1)**	**[HL]**[Yb(hfac)$_4$]·CH$_2$Cl$_2$ **(2)**
Formula	$C_{42}H_{34}N_4O_4$	$C_{62.5}H_{36}ClDyF_{24}N_4O_{10}$	$C_{63}H_{37}Cl_2YbF_{24}N_4O_{10}$
M / g.mol^{-1}	658.7	1656.9	1709.9
Crystal system	Orthorhombic	Monoclinic	Monoclinic
Space group	Pbcn (N°60)	P2$_1$/n (N°14)	C2/c (N°15)
Cell parameters	a = 13.9955(11) Å b = 15.4985(12) Å c = 15.4690(12) Å	a = 17.4236(11) Å b = 20.4734(12) Å c = 18.2388(11) Å β = 98.798(2)	a = 34.599(5) Å b = 18.712(2) Å c = 20.931(3) Å β = 100.228(3)
Volume / Å^3	3355.4(5)	6429.6(7)	13336.0(30)
Z	4	4	8
T / K	100 (2)	150(2)	150 (2)
2θ range /°	8.51 ≤ 2θ ≤ 123.88	3.01≤ 2θ ≤ 55.09	2.39 ≤ 2θ ≤ 50.28
ρ_{calc} / g.cm^{-3}	1.304	1.712	1.703
μ / mm^{-1}	0.680	1.335	1.610
Number of reflections	5974	44085	31279
Independent reflections	2981	14588	15195
R_{int}	0.0680	0.0533	0.1098
Fo^2 > 2σ(Fo)^2	2966	9504	7313
Number of variables	226	926	866
R_1, wR_2	0.0528, 0.1049	0.0677, 0.1919	0.0870, 0.2103
Compounds	(**HL**)BF$_4$·CH$_2$Cl$_2$ (**HL**)	**[HL]**[Dy(tta)$_4$] **(3)**	**[HL]**[Yb(tta)$_4$]·2.5C$_6$H$_{14}$ **(4)**
Formula	$C_{43}H_{33}BCl_2F_4N_4O_2$	$C_{74}H_{46}DyF_{12}N_4O_{10}S_4$	$C_{89}H_{82}YbF_{12}N_4O_{10}S_4$
M / g.mol^{-1}	795.4	1669.9	1896.9
Crystal system	Triclinic	Triclinic	Triclinic
Space group	P-1 (N°2)	P-1 (N°2)	P-1 (N°2)
Cell parameters	a = 10.7033(9) Å b = 12.9516(9) Å c = 14.5254(11) Å α = 74.590(3) β = 72.866(3) γ = 79.433(3)	a = 15.559(8) Å b = 16.523(9) Å c = 18.625(7) Å α = 69.035(19) β = 88.660(20) γ = 72.820(20)	a = 15.5976(15) Å b = 17.2499(19) Å c = 18.4895(19) Å α = 69.910(4) β = 88.405(5) γ = 69.699(8)
Volume / Å^3	1842.9(2)	4253.0(40)	4326.4(8)
Z	2	2	2
T / K	150(2)	150(2)	150(2)
2θ range /°	3.01 ≤ 2θ ≤ 55.01	2.35 ≤ 2θ ≤ 50.28	2.38≤ 2θ ≤ 55.08
ρ_{calc} / g.cm^{-3}	1.433	1.304	1.456
μ / mm^{-1}	0.242	1.055	1.263
Number of reflections	47100	35429	47041
Independent reflections	8847	19019	18954
R_{int}	0.0793	0.1627	0.1080
Fo^2 > 2σ(Fo)^2	4728	4845	9588
Number of variables	519	885	1120
R_1, wR_2	0.0577, 0.1220	0.1511, 0.3569	0.0751, 0.1628
Compounds	**[HL]$_2$[Yb$_8$(hfac)$_{12}$(OH)$_{12}$(O)]** **·0.5C$_6$H$_{14}$·H$_2$O (5)**	**[Fe(NCS)$_2$(L)]**·CH$_3$NO$_2$ **(6)**	**[Fe(tta)(L)][Dy(tta)$_4$]** **·2.5CH$_2$Cl$_2$ (7)**
Formula	$C_{147}H_{94}Yb_8F_{72}N_8O_{42}$	$C_{45}H_{33}FeN_7O_4S_2$	$C_{84.5}H_{55}Cl_5DyFeF_{15}N_4O_{12}S_5$
M / g.mol^{-1}	5396.6	855.8	2159.2
Crystal system	Triclinic	Monoclinic	Triclinic
Space group	P-1 (N°2)	P2$_1$/a (N°14)	P-1 (N°2)
Cell parameters	a =16.3204(11) Å b = 23.8138(18) Å c = 25.4877(18) Å α = 96.480(3) β = 107.441(3) γ = 106.108(3)	a = 12.3338(5) Å b = 19.5129(9) Å c = 16.2697(7) Å β = 92.004(2)	a = 13.052(2) Å b = 18.723(3) Å c = 18.688(3) Å α = 98.069(8) β = 91.474(8) γ = 99.609(8)
Volume / Å^3	8869.3(11)	3913.2(40)	4452.5(12)
Z	2	4	2
T / K	150 (2)	150(2)	150(2)
2θ range /°	1.71 ≤ 2θ ≤ 55.16	4.87 ≤ 2θ ≤ 55.02	2.23≤ 2θ ≤ 56.21
ρ_{calc} / g.cm^{-3}	2.021	1.453	1.611
μ / mm^{-1}	4.325	0.548	1.356
Number of reflections	98417	33804	40294
Independent reflections	40665	8646	19882
R_{int}	0.0849	0.0508	0.0981
Fo^2 > 2σ(Fo)^2	21770	7599	8070
Number of variables	2245	513	1111
R_1, wR_2	0.0746, 0.1899	0.0828, 0.1653	0.1164, 0.2976

One protonated ligand, generated during the crystallization process **(HL)** crystallizes as ion pair with one [Ln(hfac)$_4$]$^-$ metallo anionic complex. **1** crystallizes in the P2$_1$/n (N°14) monoclinic space group while **2** crystallizes in the C2/c (N°15) monoclinic space group (Table 1). The asymmetric unit of **1** is composed by one molecule of **HL**, one [Dy(hfac)$_4$]$^-$ unit and one half dichloromethane molecule of crystallization (Figure 4) while **2** is composed by one molecule of **HL**, two half [Yb(hfac)$_4$]$^-$ units

and one dichloromethane molecule of crystallization (Figure S1). The Dy^{III} ion is linked to eight oxygen atoms coming from four $hfac^-$ anions. The arrangement of the ligands leads to a square antiprism (SAP, D_{4d} symmetry) coordination polyhedron from SHAPE[14] analysis (Table S1). The crystal packing reveals the formation of an organic chain of **HL** along the *b* axis. The arrangement of the ligands in **1** is very similar to the one in the molecular structure of **HL**. The 1D network of **HL** is assured by short contacts between the methoxy groups and aromatic protons (O1···H24 = 2.439 Å and O2···H27 = 2.716 Å) (Figure 5).

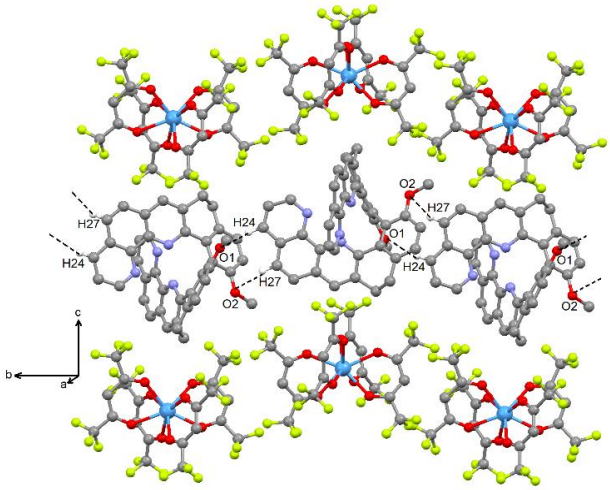

Figure 5. Crystal packing of **1** highlighting the short contacts between the ligands **HL**.

Interestingly all the ligands in the chain possess the same (S) absolute configuration. The neighbouring chain which is parallel to the bc plane has protonated ligands with opposite absolute configuration in order to form a racemic mixture in a single crystal. In the bc plane, the organic chains are isolated by $[Dy(hfac)_4]^-$ metallo units (Figure 5). Two crystallographic independent Yb^{III} sites coexist in **2**. Both ions are linked to eight oxygen atoms coming from four $hfac^-$ anions. The arrangement of the ligands leads to almost perfect square antiprism (SAP, D_{4d} symmetry) for Yb1 while an intermediate geometry is found for Yb2 from SHAPE[14] analysis (Table S1).

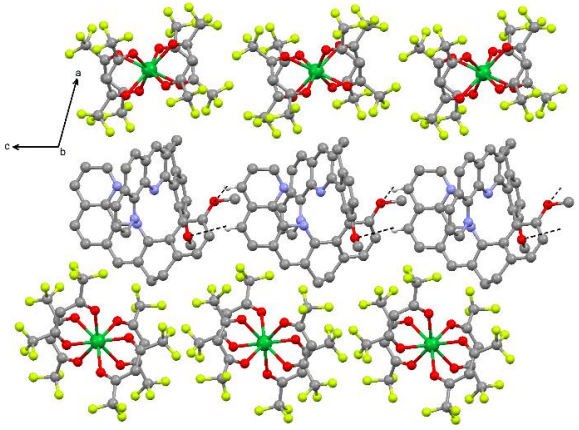

Figure 6. Crystal packing of **2** highlighting the short contacts between the ligands **HL**.

The crystal packing of **2** is also formed by one dimensional organic network of **HL** which are isolated by $[Yb(hfac)_4]^-$ metallo units. As for **1**, the 1D network of **HL** is assured by short contacts between the methoxy groups and aromatic protons (O1···H3 = 2.621 Å and O2···H6 = 2.612 Å) (Figure 6). Interestingly, contrary to **1**, the **HL** ligands in the organic chain present an alternation of their absolute configuration.

$[HL][Ln(tta)_4]\cdot nC_6H_{14}$ (Ln = Dy, n = 0 (3) and Ln = Yb, n = 2.5 (4)). Both complexes **3** and **4** have almost identical crystallographic structures. Consequently the structure description is only given for the Yb^{III} complex. **4** crystallizes in the P-1 (N°2) triclinic space group (Table 1). The asymmetric unit is composed by one molecule of **HL**, one $[Yb(tta)_4]^-$ mono-anionic complex and two and half *n*-heptane molecules of crystallization (Figures 7 and S2). The Ln^{III} ions are linked to eight oxygen atoms coming from four tta^- anions. The arrangement of the ligands leads to a square antiprism (SAP, D_{4d} symmetry) in **4** and somewhere in between D_{4d} and D_{2d} in **3** from SHAPE[14] analysis (Table S1).

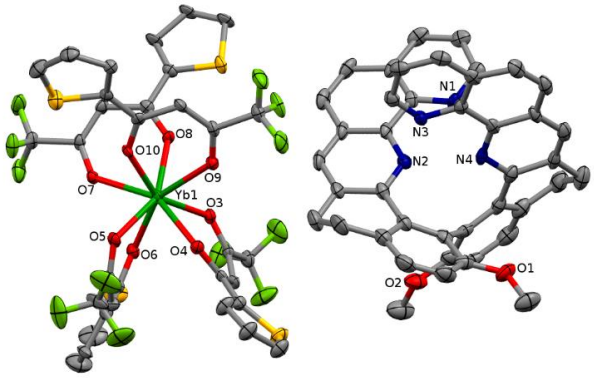

Figure 7. ORTEP view of **4**. Thermal ellipsoids are drawn at 30% probability. Hydrogen atoms and *n*-heptane molecule of crystallization are omitted for clarity. Colour code: grey, carbon atoms; red, oxygen atoms; blue, nitrogen atoms; green, fluoride atoms; dark green, ytterbium atom; yellow, sulfur atoms.

The substitution of the $hfac^-$ ancillary ligands with tta^- ones drastically changes the crystal packing. The two $[Ln(tta)_4]^-$ anions and the **HL** ligand interact through π-π interactions between the phenantroline and tta^- moieties. The chiral ligands do not form one-dimensional networks but isolated dimers in which the two ligands (**HL**) have opposite absolute configuration (Figure S3).

$[HL]_2[Yb_8(hfac)_{12}(OH)_{12}(O)]\cdot 0.5C_6H_{14}\cdot H_2O$ (5). **5** crystallizes in the P-1 (N°2) triclinic space group (Table 1). The asymmetric unit is composed by two molecules of **HL**, one cluster of eight Yb^{III} ions, one half *n*-heptane molecule and one water molecule of crystallization (Figure 8). An ORTEP view of **5** is depicted in Figure S4. In the octanuclear cluster, two kinds of Yb^{III} ions can be distinguished:the four central Yb^{III} ions (Yb3, Yb4, Yb5 and Yb6) are linked to one $hfac^-$ anion and are connected by a μ_4-O oxo dianion while the other four Yb^{III} ions (on the top Yb1 and Yb2, on the bottom Yb7 and Yb8) are linked to two $hfac^-$ anions (Figure S5). All the Yb^{III} ions are connected by 12 μ_3-OH hydroxo anions. Consequently all the Yb^{III} are eight coordinated in an O8 environment but three different symmetries of the coordination sphere can be identified i.e. triangular dodecahedron (D_{2d}) for Yb1 and Yb2; biaugmented trigonal prism (C_{2v}) for Yb3, Yb4, Yb5, Yb6 and Yb7; and square antiprism (D_{4d}) for

Yb8 (Table S1).

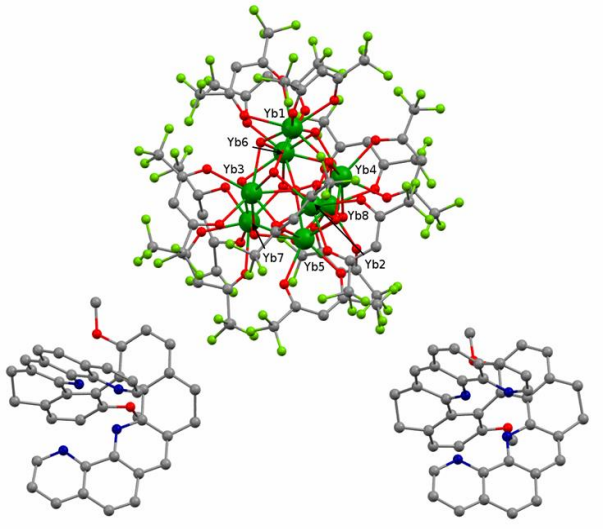

Figure 8. Molecular structure of **5**. Colour code: grey, carbon atoms; red, oxygen atoms; blue, nitrogen atoms; green, fluoride atoms; dark green, ytterbium atoms.

The formation of an octanuclear complex instead of a mononuclear one is due to the presence of base in the synthesis allowing the formation of hydroxides. **5** is a dianionic species and so two protonated **HL** ligands are present in the asymmetric unit. The crystal packing reveals π-π interactions between the phenantroline moieties leading to the formation of both one-dimensional organic network of **HL** and an inorganic network of octanuclear complexes along the *a* axis (Figure S6). It is worth noticing that in the 1D organic network the **HL** ligands have alternating absolute configurations due to the presence of an inverse centre.

$[Fe(NCS)_2(L)]\cdot CH_3NO_2$ (6). Since we were not able to coordinate 4f elements with the **L** ligand, the coordination chemistry of Fe^{II} ion was explored.

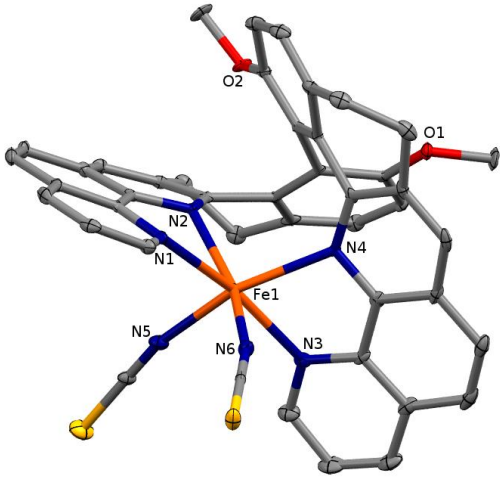

Figure 9. ORTEP view of **6**. Thermal ellipsoids are drawn at 30% probability. Hydrogen atoms and nitromethane molecule of crystallization are omitted for clarity. Colour code: grey, C atoms; red, oxygen atoms; blue, nitrogen atoms; yellow, sulphur atoms; orange, iron atom.

In order to obtain interesting magnetic properties, the $Fe(NCS)_2$ precursor was used to obtain a mononuclear complex of Fe^{II} which can potentially display spin crossover behaviour when it is associated to two nitrogenated bischelating ligands.[15] **6** crystallizes in the $P2_1/a$ (N°14) monoclinic space group (Table 1). The asymmetric unit is composed by one molecule of $[Fe(NCS)_2(\mathbf{L})]$ and one nitromethane (CH_3NO_2) molecule of crystallization (Figure 9). The Fe^{II} ion lies in a distorted N6 octahedral coordination sphere. The nitrogen atoms come from two thiocyanate anions (N5 and N6) and two phenantroline fragments (N1, N2 and N3, N4). The average Fe-N distance is 2.217 Å with the Fe-N_{NCS} bond lengths (2.113 Å) which are slightly shorter than the Fe-N_{phen} bond lengths (2.269 Å). This observation can be explained by the anionic character of the thiocyanate as well as by the constraints imposed by **L**. The average Fe-N bond length is compatible with a high-spin state Fe^{II} ion (S = 2) at 150 K. The crystal packing highlights only van der Waals contacts between the molecules (Figure S7).

$[Fe(tta)(L)][Dy(tta)_4]\cdot 2.5CH_2Cl_2$ (7). The previous X-ray structures have shown the possibility to associate the **HL** ligand with a lanthanide precursor while the **L** ligand can coordinate a Fe^{II} ion. The association of both Fe^{II} and 4f ions with **L** is now explored. The X-ray structure of **7** highlights the presence of both Dy^{III} and Fe^{II} ions and confirms that the Fe^{II} remains coordinated to **L** after addition of $Dy(tta)_3\cdot 2H_2O$. **7** crystallizes in the P-1 (N°2) triclinic space group (Table 1). The asymmetric unit is composed by one cationic molecule of $[Fe(tta)(\mathbf{L})]^+$, one anionic molecule of $[Dy(tta)_4]^-$ and two and half dichloromethane (CH_2Cl_2) molecules of crystallization (Figure 10).

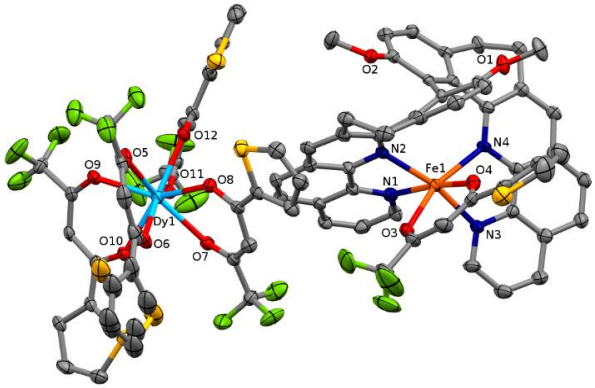

Figure 10. ORTEP view of **7**. Thermal ellipsoids are drawn at 30% probability. Hydrogen atoms and dichloromethane molecule of crystallization are omitted for clarity.

The Dy^{III} ion is linked to eight oxygen atoms coming from four tta^- anions. The arrangement of the ligands leads to an intermediate coordination polyhedron between a square antiprism (SAP, D_{4d} symmetry) and a trigonal dodecahedron (TD, D_{2d} symmetry) from SHAPE[14] analysis. Four nitrogen atoms and two oxygen atoms constitute the first coordination sphere of the Fe^{II} ion that leads to a distorted octahedral geometry. The nitrogen atoms come from the tetradentate ligand **L** whereas the two oxygen atoms come from the tta^- anion. The Fe-N distances (2.201(10) Å) are longer than the Fe-O distances (2.083(9) Å) and they are in agreement with a high-spin state Fe^{II} ion. Starting from the $Fe(NCS)_2$ precursor the same final product crystallizes giving us confidence in the fact that the driving force of the formation of the 3*d*4*f* heterobimetallic compound **7** is the formation of the

$[Dy(tta)_4]^-$ anion assisted by the labile ancillary tta^- ligands.[16]
The crystal packing highlights an alternating organization of the anions and cations without formation of anionic or cationic networks as it was observed for compounds **1**, **2** and **5** (Figure S8).
The structural analysis of the series of compounds has led to some conclusions: i) the nature of the lanthanide ions drives the molecular arrangement: homochiral 1D networks of **HL** is observed in **1** (obtained from Dy^{III} ion) while an heterochiral 1D network of **HL** is obtained in **2** (obtained from Yb^{III} ion); ii) the dimensionality of the **HL** network depends on the nature of the ancillary ligands: for $hfac^-$ (in **1** and **2),** 1D network is observed while when tta^- is used (in **3** and **4) only** isolated **HL** ligands are observed ; iii) the nuclearity of Ln complexes changes depending on the presence of base or not: mononuclear compounds (**4**) are obtained without base while an octanuclear compound (**5**) is obtained in presence of Et_3N; finally iv) the ligand **L** is able to coordinate 3*d* ions but 3*d*4*f* heterobimetallic compounds can be obtained as alternated ion pairs.

Photophysical analysis

Absorption properties

The UV-visible absorption properties of **HL** have been studied in a CH_2Cl_2 solution (Figure 11a), rationalized by TD-DFT calculations (Figure 11b) and the molecular orbital diagram was determined (Figure S9).

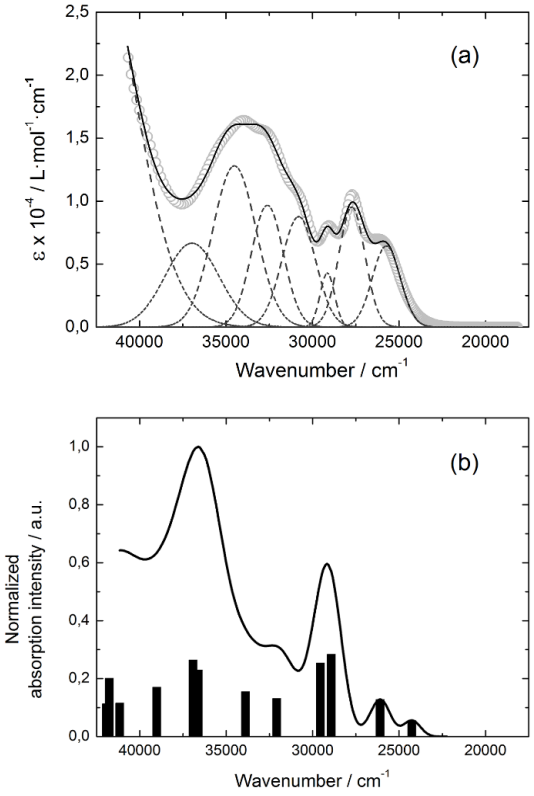

Figure 11. (a) Experimental UV-visible absorption spectra of **HL** in CH_2Cl_2 solution ($C = 4*10^{-5}$ mol·L^{-1}) (open grey circles). Respective Gaussian decompositions (dashed lines) and best fit (full black line) ($R = 0.9990$). (b) Theoretical absorption spectra of **HL** (black line). The bars represent the main contributions of the absorption spectra for **HL**.

Yb^{III} complexes **2** and **4** (Figure 12) have been studied in a CH_2Cl_2 solution. The absorption spectra of the Dy^{III} analogues (**1** and **3**) (Figure S10) as well as **5** are given in Figure S11. The experimental absorption curve of **HL** has been decomposed into eight bands (Figure 11a and Table S2). The calculated UV-visible absorption spectrum for **HL** well reproduces the experimental curve (Figure 11). Almost all the excitations have been identified as intra-ligand charge transfers from the biphenyl part of **HL** to the phenantroline part of **HL** (Table S2). In other words, the methoxy group of the biphenyl plays the role of the electron donating moieties while the phenantroline is the electron accepting group. The absorption spectrum of **HL** is completed with the intra-molecular π-π* excitations of the phenantroline moiety (HOMO-4 → LUMO +3/+4).

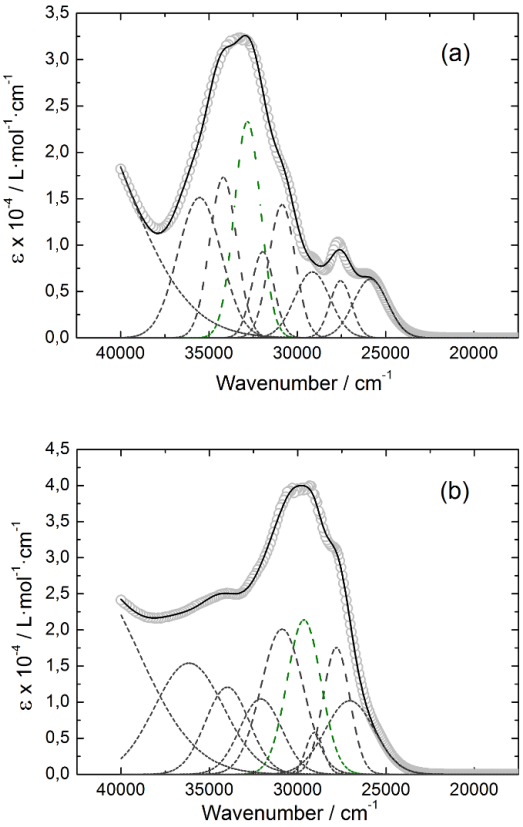

Figure 12. Experimental UV-visible absorption spectra of **2** (a) and **4** (b) in CH_2Cl_2 solution ($C = 4*10^{-5}$ mol.L^{-1}) (open gray circles). Respective Gaussian decompositions (dashed lines) and best fit (full black line) ($R = 0.9995$ for **2** and $R = 0.9988$ for **4**).

Upon complexation, a new intense absorption band at 32800 cm^{-1} for **2** and 29600 cm^{-1} for **4** is observed due to the π-π* excitations of the $hfac^-$ and tta^- ancillary ligands in the respective complexes (Figure 12).[17]

Emission properties

Emission properties of **2**, **4** and **5** were measured in solid state at room temperature (RT) and 77 K (Figures 13-15). The three Yb^{III} derivatives displayed both visible and near infrared emissions under irradiation at 28570 cm^{-1} (350 nm). The visible broad signals and infrared signals are attributed to the residual fluorescence of **HL** and Yb^{III} luminescence profile corresponding to $^2F_{5/2} \rightarrow {}^2F_{7/2}$ transitions, respectively. Lowering the temperature down to 77 K in the solid state increases the spectral resolution and allows the observation of the crystal-field splitting of the transition. The visible fluorescence is centered at 18050 cm^{-1} (RT) / 18900 cm^{-1} (77 K), 17985 cm^{-1} (RT) / 18975 cm^{-1} (77

K) and 19760 cm^{-1} (77 K) for **2**, **4** and **5**, respectively.

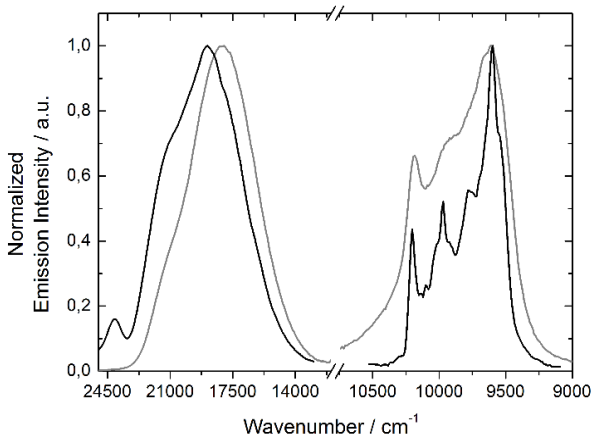

Figure 13. Solid state luminescence spectra at room temperature (gray line) and 77 K (black line) for **2** in the visible and NIR range at E_{ex} = 28570 cm^{-1} (λ_{ex} = 350 nm).

At this point, the absence of Dy-centered luminescence for compounds **1** and **3** can be explained by the too low energy of the donating level of **HL** to sensitize the Dy^{III} (17400 cm^{-1}) luminescence. Consequently only the residual visible fluorescence is observed at 20040 cm^{-1} (RT) / 21320 cm^{-1} (77 K) and 17985 cm^{-1} (RT) / 18485 cm^{-1} (77 K) respectively for **1** and **3** (Figures S12 and S13).

For **2**, four main contributions are identified in the emission spectrum of the Yb^{III} ion, which are centred at 10204, 9970, 9785 and 9597 cm^{-1} (Figure 13). Some shoulders seem to be also present in this spectrum. These could be attributed to the presence of two crystallographically independent Yb^{III} ions with slightly different coordination polyhedra and/or vibrational contributions and/or transitions coming from excited M_J states of the $^2F_{5/2}$ multiplet state.[18]

In addition, looking at lower energy an additionnal emision has been detected at 7825 cm^{-1} (1278 nm) (Figure 14). It can be attributed to a singlet oxygen phosphorescence ($a^1\Delta_g \rightarrow X^3\Sigma_g^-$) as evidence by a direct by a direct comparison with the signal obtained upon excitation of a phenalenone solution (figure SXX), a classical singlet oxygen sensitizer.[19] Similar sensitization have already been observed with related coordination complexes[20] and recently with an ytterbium derivative[21]

This emission has been revealed important in fields that range from atmospheric chemistry and materials science to biology and medicine.[22]

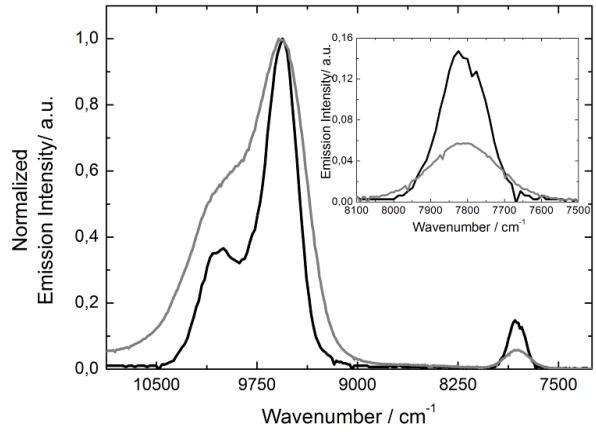

Figure 14. Luminescence spectra at room temperature (gray line) and 77 K (black line) in the solid state for **2** in the NIR range at E_{ex} = 28570 cm^{-1} (λ_{ex} = 350 nm).

For **4**, five main contributions are identified in the emission spectrum of the Yb^{III} ion which are centered at 10223, 10028, 9986, 9798 and 9662 cm^{-1} (Figure 15). This number of contributions is higher than the degeneracy of the $^2F_{7/2}$ ground state (Kramer's doublets) (maximum 4 contributions). By analogy with some of our previous work[5e],[5f],[23] and the one by Auzel et al.[24], the additional emission contributions could be attributed to transitions coming from the second and/or third M_J states of the $^2F_{5/2}$ multiplet state and/or vibrational contribution but not from the existence of different Yb^{III} ions since the crystal structure of **4** highlights only one crystallographically independent metal center.

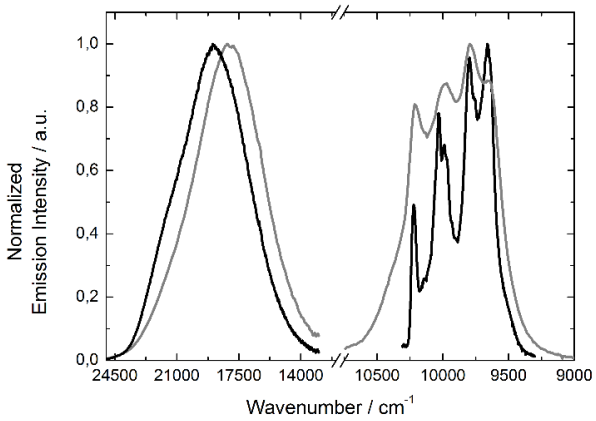

Figure 15. Solid State luminescence spectra at room temperature (gray line) and 77 K (black line) for **4** in the visible and NIR range at E_{ex} = 28570 cm^{-1} (λ_{ex} = 350 nm).

Finally for **5**, the near infrared luminescence spectrum is less resolved than for **2** and **5** but still four contributions can be observed at 10204, 9980, 9833 and 9708 cm^{-1} (Figure S14). Several parameters allow to explain the low resolution and intensity of the signal: i) self-quenching due to the proximity of eight Yb^{III} ions; ii) quenching of the luminescence by the OH^- bridges in the structure; iii) broadening of the contributions due to the eight crystallographically independent Yb^{III} ions with different coordination polyhedra.

Magnetic Properties.

The $\chi_M T$ *vs.* T (where χ_M is the molar magnetic susceptibility and T the temperature in kelvin) have been recorded for all the compounds between 2 and 300 K. For compounds **1**-**4** the $\chi_M T$ *vs.* T curves are represented in Figure 16. At room temperature, $\chi_M T$ is equal to 14.15, 2.19, 13.93 and 2.35 cm^3 K mol^{-1} for **1**, **2**, **3** and **4** respectively. $\chi_M T$ decreases monotonically on cooling down for all compounds to reach 10.7, 0.97, 10.22 and 1.2 cm^3 K mol^{-1} at 2 K for **1**, **2**, **3** and **4** respectively. Room temperature values are in agreement with the $^6H_{15/2}$ and $^2F_{7/2}$ multiplet ground-state of isolated Dy^{III} (expected 14.14 cm^3 K mol^{-1}) and Yb^{III} (expected 2.57 cm^3 K mol^{-1}) ions.[25] The decrease at low temperature is due to the thermal

depopulation of the crystal field sublevels. The magnetization curves at 2 K are represented in Figure S15.

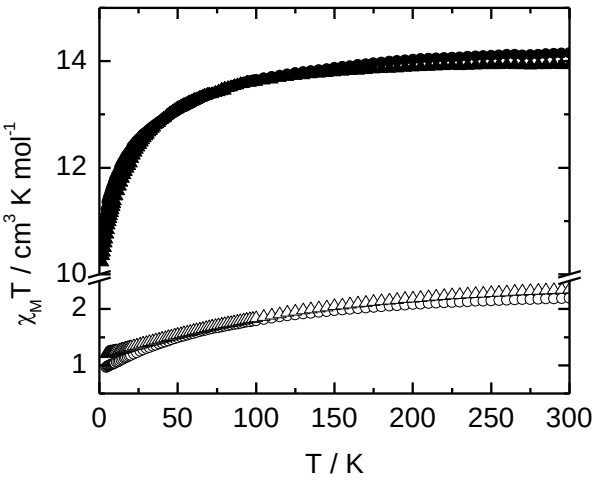

Figure 16. Temperature variation of $\chi_M T$ for **1** (●), **2** (○), **3** (▲) and **4** (△).

The absence of saturation of the magnetization at a value close to 5 Nβ for Dy^{III} derivatives indicates that the Kramer ground-state is not only constituted of the pure Ising $M_J=\pm15/2$ components. None of these compounds show non-negligible positive out-of-phase signal of the ac susceptibility in zero external dc field, whatever the frequency of the ac field and the temperature.

The $\chi_M T$ room temperature value for compound **5** is equal to 17.1 cm^3 K mol^{-1} (Figure S16). It is slightly lower than the expected value for **8** uncoupled Yb^{III} magnetic moments (20.6 cm^3 K mol^{-1}). $\chi_M T$ decreases continuously on cooling to reach 8.5 cm^3 K mol^{-1} at 2 K. At 2 K, the magnetization does not reach saturation at 50 kOe (12.6 Nβ, Figure S17). No interactions (ferromagnetic or antiferromagnetic) can be detected down to 2 K.

The Fe^{II} complex (**6**) is high-spin (S = 2) with a room temperature $\chi_M T$ value equal to 2.7 cm^3 K mol^{-1} (Figure S18). On cooling $\chi_M T$ decreases slightly (Figure S18) as expected from the effect of zero-field splitting on the ground state, but no spin transition is observed.

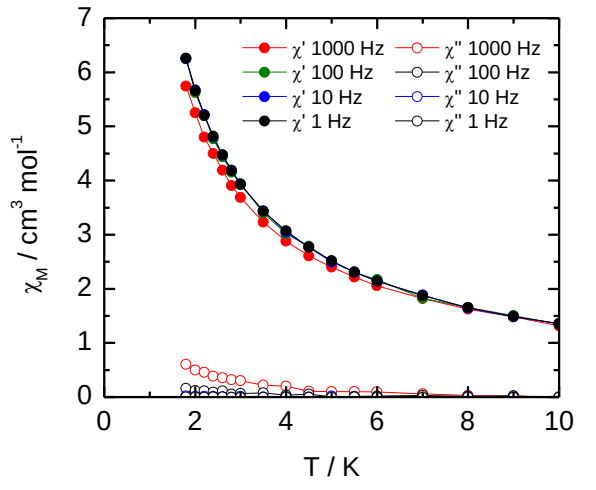

Figure 17. Temperature dependence of the in-phase (χ') and out-of-phase (χ'') components of the ac susceptibility measured on **7** between 2 and 10 K at zero external dc field.

At room temperature the value of $\chi_M T$ for compound **7** is equal to 16.7 cm^3 K mol^{-1} which is close to the value expected for an isolated Fe^{II} high-spin (3.0 cm^3 K mol^{-1}) plus an isolated Dy^{III} centre (14.17 cm^3 K mol^{-1}) (Figure S19). $\chi_M T$ decreases on cooling as expected. No saturation of the magnetization occurs at 2 K (Figure S17). Amazingly, the ac susceptibility at low temperature reflects a Single-Molecule Magnet (SMM) behaviour. Indeed, even in zero external dc field, an out-of-phase signal, χ_M'' is detected at 2 K which is typically due to the slow relaxation of the magnetic moment of Dy^{III} in a D_{4d} environment (Figure 17).[2c] The maximum on the χ_M'' vs. ν curves migrates progressively to the low frequency side with the increase of the external dc field with an evident broadening which can be attributed to an in-field contribution from Fe^{II} centres (Figure S20). In the absence of any specific investigations of the ac susceptibility on isolated high spin Fe^{II} complex found in **7** we cannot extract quantitative information on the relaxation processes. Interestingly, $[Dy(tta)_4]^-$ relax in zero field while $[Dy(hfac)_4]^-$ does not. This can be due to the fact that oxygen atoms are more negatively charged in tta^- ligand than in $hfac^-$.[26]

Conclusions

In the present article, a new chiral helicene-like ligand (**L**) was synthesized as well as its protonated form (**HL**). X-ray structures revealed drastic structural changes between the two forms. Starting from the neutral form, its association with the $Ln(hfac)_3$ and $Ln(tta)_3$ metallo-precursor leads to its spontaneous protonation and the design of five complexes $[\mathbf{HL}][Ln(hfac)_4]\cdot nCH_2Cl_2$(Ln = Dy, n = 0.5 (**1**) and Ln = Yb, n = 1 (**2**)), $[\mathbf{HL}][Ln(tta)_4]\cdot nC_6H_{14}$ (Ln = Dy, n = 0 (**3**) and Ln = Yb, n = 2.5 (**4**) and $[\mathbf{HL}]_2[Yb_8(hfac)_{12}(OH)_{12}(O)]\cdot 0.5C_6H_{14}\cdot H_2O$ (**5**). No protonation of the ligand is observed in presence of Fe^{II} ion with the formation of the $[Fe(NCS)_2(\mathbf{L})]\cdot CH_3NO_2$ (**6**) complex. Finally a 3*d*4*f* heterobimetallic of formula $[Fe(tta)(\mathbf{L})][Dy(tta)_4]\cdot 2.5CH_2Cl_2$ (**7**) was elaborated combining both Fe^{II} salt and $Dy(tta)_3$ metallo-precursor. Homochirality/heterochirality arrangement of the ligands as well as the dimension and nuclearity of the edifices depend both on the ancillary ligand nature and the presence of base during the synthesis. The absorption properties of both ligands and complexes have been experimentally studied and rationalized by TD-DFT calculations in order to optimize the light-irradiation for emission properties. The latter reveal that all the Yb^{III} analogues are emissive in the NIR region and interestingly a singlet oxygen phosphorescence is detected at 7825 cm^{-1} (1278 nm) and attributed to the infrared radiative transition of O_2 ($a^1\Delta_g \rightarrow X^3\Sigma_g^-$) for **2**. An out-of-phase signal of the magnetic susceptibility was observed for the heterobimetallic compound, the sign of single molecule magnet behaviour and efforts to better understand such system is under progress in our group. Efforts on pure enantiomeric synthesis and influence of the protonation on the chiroptical properties are currently made.

Experimental Section

Synthesis. **General Procedures and Materials**. General Procedures and Materials. The precursors $Ln(hfac)_3\cdot 2H_2O$ (Ln^{III} = Dy and Yb; $hfac^-$ = 1,1,1,5,5,5-hexafluoroacetylacetonate anion) and $Ln(tta)_3\cdot 2H_2O$ (Ln^{III} = Dy and Yb; tta^- = 2-thenoyltrifluoroacetonate anion) were synthesized following previously reported methods.[27],[28] All other reagents were purchased from Sigma-Aldrich® and used without further purification. Experiments under microwaves are run with a Biotage Initiator 2.5 microwave synthesizer.

Synthesis of the ligands

12,12'-dimethoxy-8,8',9,9'-tetrahydro-13,13'-binaphtho[1,2-b][1,10]phenanthroline (L). 8-amino-7-quinolinecarbaldehyde (0.5 g, 2.90 mmol), (±)-bis-tetralone (0.275 g, 0.78 mmol), potassium tert-butoxide (0.375 g, 3.34 mmol) in THF (12 mL) are stirred at 70°C for 5 hours under microwave irradiation (average absorption). After cooling and evaporation of the THF, the crude was diluted with CH_2Cl_2 and washed twice with H_2O. A first purification is done by silica gel column chromatography using a gradient of CH_2Cl_2/MeOH/Et_3N (100/0/0 to 90/10/1) followed by a second chromatography over neutral alumina using CH_2Cl_2/Et_3N (100/1) as eluent. If some protonation is still observed (NMR broadening of the signals), the isolated compound dissolved in CH_2Cl_2 can be deprotonated by two washing with NaOH 1M. Yield 0.38g of L (78%). Single crystals suitable for X rays crystallography are grown by slow evaporation of a solution of 20 mg of L in 5 mL of a mixture 1/1 CH_2Cl_2/Toluene.
^{1}H NMR (500.1 MHz, DMSO) δ 8.89 (dd, J = 4.01, 1.64 Hz, 1H), 8.28 (dd, J = 8.17, 1.58 Hz, 1H), 7.74 (d, J = 8.9 Hz, 1H), 7.735 (s, 1H), 7.68 (d, J = 8.9 Hz, 1H), 7.60 (dd, J = 4.2, 8.0 Hz, 1H), 7.09 (d, J = 8.3 Hz, 1H), 6.96 (d, J = 8.5 Hz, 1H), 3.11 (s, 3H), 2.47-2.32 (m 3H), 1.50 (t, J = 12.2 Hz, 1H). 13C NMR (125.75 MHz, DMSO) δ 159.51 (Cq), 155.14 (Cq), 150.11 (CH), 147.12 (Cq), 144.70 (Cq), 136.60 (CH), 134.85 5(Cq), 134.81 (Cq), 133.18 (Cq), 133.13 (CH), 129.77 (Cq), 128.83 (Cq), 127.61 (CH), 127.21 (CH), 126.84 (CH), 126.74 (CH), 123.60 (CH), 114.31 (CH), 57.25 (CH3), 29.84 (CH2). HMRS (EI) [M+H]+ calcd for [C42H30N4O2+H]+ 623.2442, meas: 623.2422.
(LH)BF_4·CH_2Cl_2 (LH). 12.4 mg of **L** (0.02 mmol) and 6.6 mg of $TBABF_4$ (0.02 mmol) are stirred in a 10 mL solution of CH_2Cl_2 for 15 min then 30 mL of *n*-hexane are layered in the dark to give yellow single crystals of LH which are suitable for X-ray diffraction study. Yield, 9.7 mg (61 %). Anal. Calcd (%) for $C_{43}H_{33}BCl_2F_4N_4O_2$: C 64.87, H 4.15, N 7.04; found: C 64.98, H 4.22 N, 7.12.
Synthesis of complexes 1-7.
[HL][Dy(hfac)$_4$]·0.5CH_2Cl_2 (1). 32.8 mg of Dy(hfac)$_3$·2H_2O (0.04 mmol) were dissolved in 10 mL of CH_2Cl_2 and then added to a solution of 5 mL of CH_2Cl_2 containing 12.4 mg of L (0.02 mmol). After 30 min of stirring, 30 mL of *n*-hexane were layered at room temperature in the dark. Slow diffusion leads to yellow single crystals, which are suitable for X-ray studies. Yield based on L, 18.9 mg (57 %). Anal. Calcd (%) for $C_{62.5}H_{36}ClDyF_{24}N_4O_{10}$: C 45.27, H 2.17, N 3.38; found: C 45.41, H 2.20 N, 3.42. I.R. (KBr): 2955, 2928, 2871, 2853, 1651, 1559, 1534, 1513, 1259, 1205, 1147, 1100, 1035, 836, 800, 662 and 587 cm^{-1}.
[HL][Yb(hfac)$_4$]·CH_2Cl_2 (2). 33.4 mg of Yb(hfac)$_3$·2H_2O (0.04 mmol) were dissolved in 10 mL of CH_2Cl_2 and then added to a solution of 10 mL of CH_2Cl_2 containing 12.4 mg of L (0.02 mmol). After 30 min of stirring, 40 mL of *n*-hexane were layered at room temperature in the dark. Slow diffusion leads to yellow single crystals, which are suitable for X-ray studies. Yield based on L, 14 mg (41 %). Anal. Calcd (%) for $C_{63}H_{37}Cl_2YbF_{24}N_4O_{10}$: C 44.21, H 2.16, N 3.28; found: C 44.29, H 2.24 N, 3.24. I.R. (KBr): 2955, 2871, 2850, 1655, 1560, 1535, 1261, 1202, 1146, 1102, 797, 663 and 589 cm^{-1}.
[HL][Dy(tta)$_4$] (3). 34.5 mg of Dy(tta)$_3$·2H_2O (0.04 mmol) were dissolved in 5 mL of CH_2Cl_2 and then added to a solution of 5 mL of CH_2Cl_2 containing 12.4 mg of L (0.02 mmol). After 30 min of stirring, 30 mL of n-hexane were layered at room temperature in the dark. Slow diffusion leads to yellow single crystals, which are suitable for X-ray studies. Yield based on L 13.4 mg (40 %). Anal. Calcd (%) for $C_{74}H_{46}DyF_{12}N_4O_{10}S_4$: C 53.18, H 2.75, N 3.35; found: C 54.05, H 2.76 N, 3.34. I.R. (KBr): 2959, 2868, 2850, 1610, 1537, 1501, 1413, 1357, 1303, 1244, 1229, 1182, 1142, 1082, 1060, 1033, 935, 832, 782, 715, 680, 643 and 580 cm^{-1}.
[HL][Yb(tta)$_4$]·2.5C_6H_{14} (4). 37.0 mg of Yb(tta)$_3$·2H_2O (0.04 mmol) were dissolved in 5 mL of CH_2Cl_2 and then added to a solution of 5 mL of CH_2Cl_2 containing 12.4 mg of L (0.02 mmol). After 15 min of stirring, 27 mL of *n*-hexane were layered at room temperature in the dark. Slow diffusion leads to yellow single crystals, which are suitable for X-ray studies. Yield based on L, 30.1 mg (79 %). Anal. Calcd (%) for $C_{89}H_{82}YbF_{12}N_4O_{10}S_4$: C 56.30, H 4.32, N 2.95; found: C 56.29, H 4.39 N, 2.91. I.R. (KBr): 2955, 2928, 2870, 2850, 1612, 1538, 1502, 1414, 1358, 1309, 1247, 1230, 1183, 1142, 1061, 936, 782, 715, 643, 582 cm^{-1}.
[HL]$_2$[Yb$_8$(hfac)$_{12}$(OH)$_{12}$(O)]·0.5C_6H_{14}·H_2O (5). 33.4 mg of Yb(hfac)$_3$·2H_2O (0.04 mmol) were dissolved in 5 mL of CH_2Cl_2 and then added to a solution of 5 mL of CH_2Cl_2 containing 12.4 mg of L (0.02 mmol) and five drops of Et_3N (excess). After 15 min of stirring, 30 mL of n-hexane were layered at room temperature in the dark. Slow diffusion leads to yellow single crystals, which are suitable for X-ray studies. Yield based on the metal, 10.9 mg (10 %). Anal. Calcd (%) for $C_{147}H_{94}Yb_8F_{72}N_8O_{42}$: C 32.69, H 1.74, N 2.08; found: C 32.74, H 1.72 N, 2.04. I.R. (KBr): 3637, 2955, 2928, 2871, 2854, 1657, 1557, 1532, 1391, 1262, 1203, 1144, 1034, 832, 797, 662, 587 and 528 cm^{-1}.
[Fe(NCS)$_2$(L)]·CH_3NO_2 (6). 3.9 mg of KNCS (0.04 mmol) and 5.6 mg of $FeSO_4$·7H_2O (0.02 mmol) in presence of ascorbic acid are mixed in 3 mL of dried MeOH under argon for 30 min. Then the solution is filtered over a solution of 3 mL of CH_2Cl_2 containing 12.4 mg of L (0.02 mmol). The mixture is stirred for 15 min then concentrated and finally filtered. The collected solid is dissolved in a mixture of CH_2Cl_2/CH_3NO_2 (1:1) and slow diffusion of Et_2O offered red single crystals, which are suitable for X-ray studies. Yield 6.7 mg (39 %). Anal. Calcd (%) for $C_{45}H_{33}FeN_7O_4S_2$: C 63.10, H 3.86, N 11.45; found: C 62.89, H 3.82 N, 11.56.
[Fe(tta)(L)][Dy(tta)$_4$]·2.5CH_2Cl_2 (7). 8.0 mg of $FeCl_2$·4H_2O (0.04 mmol) were dissolved in 5 mL of degassed H_2O under argon and then 14.8 mg of solid potassium dipyrazolhydroborate KH_2Bpz_2 (0.04 mmol)[29] were added in one portion under stirring. The light yellow solid formed was dissolved by addition of 5 mL of CH_2Cl_2. The aqueous phase was removed and the organic one was dried with $MgSO_4$. A solution of 5 mL of CH_2Cl_2 containing 12.4 mg of L (0.02 mmol) was added to the organic phase and the resulting solution stirred for 15 min. Then 5 mL of CH_2Cl_2 containing 17.3 mg of Dy(tta)$_3$·2H_2O (0.02 mmol) were added. After 15 min of stirring, 20 mL of *n*-hexane were layered at room temperature in the dark. Slow diffusion leads to purple single crystals, which are suitable for X-ray studies. Yield 14.3 mg (33 %). Anal. Calcd (%) for $C_{84.5}H_{55}Cl_5DyFeF_{15}N_4O_{12}S_5$: C 46.96, H 2.55, N 2.59; found: C 47.09, H 2.61 N, 2.60. I.R. (KBr): 2955, 2929, 2870, 2850, 1610, 1536, 1506, 1414, 1356, 1305, 1245, 1229, 1181, 1138, 1060, 1034, 935, 781, 714, 681, 643 and 581 cm^{-1}. This compound can be obtained using the experimental protocol of **6** followed by the addition of 2 equivalents of Dy(tta)$_3$·2H_2O and crystallization by diffusion of *n*-hexane in a CH_2Cl_2 solution.
Crystallography. A single crystal of **L** was mounted on an Oxford Diffractometer for data collection (MoKα radiation source, λ = 0.71073 Å, T = 100 K) while **HL**·BF_4 and complexes **1**-**7** were mounted on an APEXII Bruker-AXS diffractometer for data collection (MoKα radiation source, λ = 0.71073 Å, T = 150 K), from the Centre de Diffractométrie (CDIFX), Université de Rennes 1, France. Structures were solved with a direct method using the SIR-97 program and refined with a full matrix least-squares method on F2 using CRYSTALS and SHELXL-97 programs.[30] Crystallographic data are summarized in Table 1. Complete crystal structure results as a CIF file including bond lengths, angles, and atomic coordinates are deposited as Supporting Information. The crystal quality and data for compounds 3 and 7 was not very good. Other attempts of crystallization were done but not better quality crystals were found and after several attempts of data collection, the reported ones were found to be the best ones.
Physical Measurements. The elementary analyses of the compounds were performed at the Centre Régional de Mesures Physiques de l'Ouest, Rennes. 1H and 13C NMR were recorded on a Bruker Avance II 500 spectrometer. Chemical shifts are reported in parts per million referenced to TMS for ^{1}H NMR. Mass spectrometry (HRMS, LSIMS) was performed at the Centre de Spectrométrie de Masse, Université de Lyon, France. Absorption spectra were recorded on a Varian Cary 5000 UV-Visible-NIR spectrometer equipped with an integration sphere. The luminescence spectra were measured using a Horiba-Jobin Yvon Fluorolog-3® spectrofluorimeter, equipped with a three slit double grating excitation and emission monochromator with dispersions of 2.1 nm/mm (1200 grooves/mm). The steady-state luminescence was excited by unpolarized light from a 450 W xenon CW lamp and detected at a 90° angle by a red-sensitive Hamamatsu R928 photomultiplier tube. Spectra were reference corrected for both the excitation source light intensity variation (lamp and grating) and the emission spectral response (detector and grating). Near infra-red spectra were recorded at a 90° angle using liquid nitrogen cooled, solid indium/gallium/arsenic detector (850-1600 nm). Solid state measurements are performed in quartz tube. The dc magnetic susceptibility measurements were performed on solid polycrystalline sample with a Quantum Design MPMS-XL SQUID magnetometer between 2 and 300 K in applied magnetic field of 0.2 T for temperatures of 2-20 K and 1T for temperatures of 20-300 K. These measurements were all corrected for the diamagnetic contribution as calculated with Pascal's constants.
Computational Details. DFT geometry optimizations and TD-DFT excitation energy calculations of the ligand HL were carried out with the Gaussian 09 (revision A.02) package[31] employing the PBE0 hybrid functional.[32] All atoms were described with the SVP basis sets.[33] The first 50 monoelectronic excitations were calculated. In all steps, a modelling of bulk solvent effects (solvent = dichloromethane) was included through the Polarisable Continuum Model (PCM),[34] using a linear-response non-equilibrium approach for the TD-DFT step.[35] Molecular orbitals were sketched using the Gabedit graphical interface.[36]

Supporting Information (see footnote on the first page of this article): Ortep views for 2 (Figure S1), 3 (Figure S2), 5 (Figure S4), packing views for 4 (Figure S3), 5 (Figure S6), 6 (Figure S7), 7 (Figure S8), additional photo-physical measurements for 1 (Figures S9 and S10), 3 (Figure S11), additional magnetic measurements (Figure S12-S17), SHAPE data (Table S1). Complete crystal structure results as a CIF file including bond lengths, angles, and atomic coordinates are deposited as Supporting Information. CCDC 1509188-1509196 contain the supplementary crystallographic data for all the compounds. These data can be obtained free of charge from the Cambridge Crystallographic Data Centre via www.ccdc.cam.ac.uk/data_request/cif)

Acknowledgments

This work was supported by the CNRS, Rennes Métropole, Université de Rennes 1, Région Bretagne, FEDER, ENS Lyon, Université Claude Bernard Lyon 1 and Agence Nationale de la Recherche (N° ANR-13-BS07-0022-01). B.L.G. thanks the French GENCI-CINES center for high-performance computing resources (project x2015080649).

[1] a) P. Gütlich, Y. Garcia, H. A. Goodwin, *Chem. Soc. Rev.* **2000**, *29*, 419−427; b) A. Bousseksou, G. Molnar, L. Salmon, W. Nicolazzi, *Chem. Soc. Rev.* **2011**, *40*, 3313−3335; c) M. C. Munoz, J. A. Real, *Coord. Chem. Rev.*, 2011, **255**, 2068−2093; d) G. Aromí, L. A. Barrios, O. Roubeau, P. Gamez, *Coord. Chem. Rev.* **2011**, *255*, 485−546; e) M. A. Halcrow, *Chem. Soc. Rev.* **2011**, *40*, 4119−4142.

[2] a) R. Sessoli, D. Gatteschi, A. Caneschi, M. A. Novak, *Nature* **1993**, *365*, 141-143; b) G. Aromi, E. K. Brechin, in Single-Molecule Magnets and Related Phenomena, ed. R. Winpenny, 2006, pp. 1–67; c) D. N. Woodruff, R. E. P. Winpenny, R. A.

Layfield, *Chem. Rev*. **2013**, *113*, 5110-5148; d) J. M. Frost, K. L. M. Harriman, M. Murugesu, *Chem. Sci.* **2016**, *7*, 2470-2491.

[3] a) L. Bogani, W. Wernsdorfer, *Nat. Mater*. **2008**, *7*, 179-186; b) M. N. Leuenberger, D. Loss, *Nature* **2001**, *410*, 789-793; c) J. Lehmann, A. Gaita-Arino, E. Coronado, D. Loss, *J. Mater. Chem.* **2009**, *19*, 1672-1677; d) J. Camarero, E. Coronado, *J. Mater. Chem.* **2009**, *19*, 1678-1684; e) O. Kahn, C. J. Martinez, *Science* **1998**, *279*, 44-48.

[4] a) C. Train, R. Gheorge, V. Krstic, L.-M. Chamoreau, N. S. Ovanesyan, G. L. J. A. Rikken, M. Gruselle, M. Verdaguer, *Nat. Mat.* **2008**, *7*, 729-734; b) C. Train, M. Gruselle, M. Verdaguer, *Chem. Soc. Rev*. **2011**, *40*, 3297-3313.

[5] a) M.-E. Boulon, G. Cucinotta, J. Luzon, C. Degl'Innocenti, M. Perfetti, K. Bernot, G. Calvez, A. Caneschi, R. Sessoli, *Angew. Chem. Int. Ed.* **2013**, *52*, 350-354; b) G. Cucinotta, M. Perfetti, J. Luzon, M. Etienne, P. E. Car, A. Caneschi, G. Calvez, K. Bernot, R. Sessoli, *Angew. Chem. Int. Ed.* **2012**, *51*, 1606-1610; c) M. Ren, S.-S. Bao, R. A. S. Ferreira, L.-M. Zheng, L. D. Carlos, *Chem. Commun.* **2014**, *50*, 7621-7624; d) F. Pointillart, B. Le Guennic, S. Golhen, O. Cador, O. Maury, L. Ouahab, *Chem. Commun.* **2013**, *49*, 615-617; e) K. Soussi, J. Jung, F. Pointillart, B. Le Guennic, B. Lefeuvre, S. Golhen, O. Cador, Y. Guyot, O. Maury, L. Ouahab, *Inorg. Chem. Front.* **2015**, *2*, 1105-1117; f) X. Yi, K. Bernot, V. Le Corre, G. Calvez, F. Pointillart, O. Cador, B. Le Guennic, J. Jung, O. Maury, V. Placide, Y. Guyot, T. Roisnel, C. Daiguebonne, O. Guillou, *Chem. Eur. J.* **2014**, *20*, 1569-1576; g) T.-Q. Liu, P.-F. Yan, F. Luan, Y.-X. Li, J.-W. Sun, C. Chen, F. Yang; H. Chen, X.-Y. Zou, G.-M. Li, *Inorg. Chem.* **2015**, *54*, 221-228; h) K. S. Pedersen, J. Dreiser, H. Weihe, R. Sibille, H. V. Johannesen, M. A. Sorensen, B. E. Nielsen, M. Sigrist, H. Mutka, S. Rols, J. Bendix, S. Piligkos, *Inorg. Chem.* **2015**, *54*, 7600-7606; i) Q.-W. Li, J.-L. Liu, J.-H. Jia, Y.-C. Chen, J. Liu, L.-F. Wang, M.-L. Tong, *Chem. Commun.* **2015**, *51*, 10291-10294; j) W. Huang, J. Xu, D. Wu, X. Huang, J. Jiang, *New J. Chem.* **2015**, *39*, 8650-8657.

[6] a) J. Long, J. Rouquette, J.-M. Thibaud, R. A. S. Ferreira, L. D. Carlos, B. Donnadieu, V. Vieru, L. F. Chibotaru, L. Konczewicz, J. Haines, Y. Guari, J. Larionova, *Angew. Chem., Int. Ed.* **2015**, 54, 2236–2240; b) G. Novitchi, G. Pilet, L. Ungur, V. V. Moshchalkov, W. Werndorfer, L. F. Chibotaru, D. Luneau, A. K. Powell, *Chem. Sci.* **2012**, *3*, 1169-1176.

[7] a) J. Bosson, J. Gouin, J. Lacour, *Chem. Soc. Rev*. **2014**, *43*, 2824-2840; b) N. Saleh, C. Shen, J. Crassous, *Chem. Sci.* **2014**, 5, 3680-3694; b) C. Shen, E. Anger, M. Srebro, N. Vanthuyne, K. K. Deol, T. D. Jefferson Jr., G. Muller, J. A. G. Williams, L. Toupet, C. Roussel, J. Autschbach, R. Réau, J. Crassous, *Chem. Sci.* **2014**, *5*, 1915-1927; c) K. Nakamura, S. Furumi, M. Takeuchi, T. Shibuya, K. Tanaka, *J. Am. Chem. Soc.* **2014**, *136*, 5555-5558; d) V. I. Lindell, A. Shivola, S. Tretyakov, A. Viitanen, Electromagnetic waves in Chiral and Bi-Isotropic Media; Artech House: **1994**; e) J. Mazur, M. Mrozowski, M. Okoniewski, *JEWA*, **1992**, 5-6, 641-650; f) S. Guy, A. Bensal-Ledoux, A. Stoita-Crisan, *PIER B*, **2010**, *24*, 155-172; g) M. Krykunov, M. D. Kundrat, J. J. Autschbach, *Chem. Phys.* **2006**, *125*, 194110.

[8] a) S. D. Dreher, T. J. Katz, K. C. Lam, A. L. Rheingold, *J. Org. Chem.* **2000**, *65*, 815-822; b) D. Nakano, R. Hirano, M. Yamaguchi, C. Kabuto, *Tetrahedron Lett.* **2003**, *44*, 3683-3686.

[9] a) C. Nuckolls, T. J. Katz, G. Katz, P. J. Collings, L. Castellanos, *J. Am. Chem. Soc.* **1999**, *121*, 79-88; b) S. Honzawa, H. Okubo, S. Anzai, M. Yamaguchi, K. Tsumoto, I. Kumagai, *Bioorg. Med. Chem.* **2002**, *10*, 3213-3218; c) R. Amemiya, M. Yamaguchi, *Org. Biomol. Chem.* **2008**, *6*, 26-35; d) K. Senechal-David, L. Toupet, O. Maury, H. Le Bozec, *Cryst. Growth Des.* **2006**, *6*, 1493-1496.

[10] T. Verbiest, S. Van Elshocht, A. Persoons, C. Nuckolls, K. E. Phillips, T. J. Katz, *Langmuir* **2001**, *17*, 4685-4687.

[11] C. Nuckolls, R. F. Shao, W. G. Jang, N. A. Clark, D. M. Walba, T. J. Katz, *Chem. Mater*. **2002**, *14*, 773-776.

[12] T. R. Kelly, J. P. Sestelo, I. J. Tellitu, *J. Org. Chem.* **1998**, *63*, 3655-3665.

[13] a) L. Jierry, S. Harthong, C. Aronica, J.-C. Mulatier, L. Guy, S. Guy, *Org. Lett.* **2012**, *14*, 288-291; b) A. Bensalah-Ledoux, D. Pitrat, T. Reynaldo, M. Srebro-Hooper, B. Moore, J. Autschbach, J. Crassous, S. Guy, L. Guy, *Chem. Eur. J.* **2016**, *22*, 3333.

[14] M. Llunell, D. Casanova, J. Cirera, J. M. Bofill, P. Alemany, S. Alvarez SHAPE (version 2.1), Barcelona, 2013.

[15] a) A. Galet, A. B. Gaspar, M.C. Munoz, G. Levchenko, J. A. Real, *Inorg. Chem.* **2006**, *45*, 9670-9679; b) A. Ozarowski, B. R. Mcgarvey, A. B. Sarkar, J. E. Drake, *Inorg. Chem.* **1988**, *27*, 628-635; c) T. M. Ross, B. Moubaraki, S. M. Neville, S. R. Batten, K. S. Murray, *Dalton Trans.* **2012**, *41*, 1512-1523; d) J. F. Létard, P. Guionneau, L. Rabardel, J. A. K. Howard, A. E. Goeta, D. Chasseau, O. Kahn, *Inorg. Chem.* **1998**, *37*, 4432-4441; (e) W. Vreugdenhil, J. H. Vandiemen, R. A. G. Degraaff, J. G. Haasnoot, J. Reedijk, A. M.Vanderkraan, O. Kahn, J. Zarembowitch, *Polyhedron* **1990**, *9*, 2971-2979; f) V. Legrand, S. Pillet, C. Carbonera, M. Souhassou, J. F. Létard, P. Guionneau, C. Lecomte, *Eur. J. Inorg. Chem.* **2007**, 5693-5706; g) M. Shatruk, H. Phan, B. A. Chrisostomo, A. Suleimenova, *Coord. Chem. Rev*. **2015**, *289-290*, 62-73.

[16] F. Pointillart, T. Guizouarn, B. Lefeuvre, S. Golhen, O. Cador, L. Ouahab, *Chem. Eur. J.* **2015**, *21*, 16929-16934.

[17] F. Pointillart, J. Jung, R. Berraud-Pache, B. Le Guennic, V. Dorcet, S. Golhen, O. Cador, O. Maury, Y. Guyot, S. Decurtins, S.-X. Liu, L. Ouahab, *Inorg. Chem.* **2015**, *54*, 5384-5397.

[18] a) W. Tian, L. Deng, S. Jin, H. Yang, R. Cui, Q. Zhang, W. Shi, C. Zhang and X. Yuan, G. Sha, *J. Phys. Chem. A.* **2015**, *119*, 3393-3399; b) T. Gallavardin, M. Maurin, S. Marotte, T. Simon, A.-M. Gabudean, Y. Bretonnière, M. Lindgren, F. Lerouge, P. L. Baldeck, O. Stéphan, Y. Leverrier, J. Marvel, S. Parola, O. Maury, C. Andraud *Photochem. & Photobiol. Science* **2011**, *10*, 1216-1225.

[19] a) R. Schmidt, C. Tanielian, R. Dunsbach, C. Wolff, *J. Photochem.Photobiol. A*, **1994**, *79*, 11-17. b) T. Gallavardin, M. Maurin, S. Marotte, T. Simon, A.-M. Gabudean, Y. Bretonnière, M. Lindgren, F. Lerouge, P. L. Baldeck, O. Stéphan, Y. Leverrier, J. Marvel, S. Parola, C., O. Maury, Andraud *Photochem. & Photobiol. Science* **2011**, *10*, 1216-1225.

[20] [R. M. Spada, M. Cepeda-Plaza, M. L. Goméz, G. Günther, P. Jaque, N. Pizarro, R. E. Palacios, A Vega, *J. Phys. Chem. C* **2015**, *119*, 10148−10159]

[21] [A. Watkis, R. Hueting, T. J. Sørensen, M. Tropiano, S. Faulkner Chem. Commun. **2015**, *51*, 15633-15636]

[22] P. R. Ogilby, *Chem. Soc. Rev*. **2010**, *39*, 3181-3209.

[23] a) G. Cosquer, F. Pointillart, J. Jung, B. Le Guennic, S. Golhen, O. Cador, Y. Guyot, A. Brenier, O. Maury, L. Ouahab, *Eur. J. Inorg. Chem.* **2014**, 69–82; b) J. Jung, T. da Cunha, B. Le Guennic, F. Pointillart, L. M. Pereira, J. Luzon, S. Golhen, O. Cador, O. Maury, L. Ouahab, *Eur. J. Inorg. Chem.* **2014**, 3888-3894.

[24] P. Goldner, F. Pellé, D. Meichenin, F. Auzel, *J. Lumin.* **1997**, *71*, 137–150.

[25] O. Kahn, Molecular Magnetism, VCH: Weinhem, 1993.

[26] T. T. da Cunha, J. Jung, M.-E. Boulon,G. Campo, F. Pointillart,C. L. M.Pereira,B. Le Guennic, O. Cador, K. Bernot, F. Pineider, S. Golhen, L. Ouahab, *J. Am. Chem. Soc.* **2013**, *135*, 16332–16335.

[27] M. F. Richardson, W. F. Wagner, D. E. Sands, *J. Inorg. Nucl. Chem.* **1968**, *30*, 1275-1289.

[28] A. I. Vooshin, N. M. Shavaleev, V. P. Kazakov, *J. Luminescence* **2000**, *91*, 49-58.

[29] S. Trofimenko, *J. Am. Chem. Soc*. **1967**, *89*, 3170-3177.

[30] a) SHELX97 - Programs for Crystal Structure Analysis (Release 97-2). G. M. Sheldrick, Institut für Anorganische Chemie der Universität, Tammanstrasse 4, D-3400 Göttingen, Germany, 1998. SIR97 – A. Altomare, M. C. Burla, M. Camalli, G. L. Cascarano, C. Giacovazzo, A. Guagliardi, A. G. G. Moliterni, G. Polidori, R. Spagna, *J. Appl. Cryst.* **1999**, *32*, 115-119; (b) P. W. Betteridge, J. R. Carruthers, R. I. Cooper, K. Prout, D. J. Watkin, *J Appl. Cryst.* **2003**, *36*, 1487.

[31] M. J. Frisch, G. W. Trucks, H. B. Schlegel, G. E. Scuseria, M. A. Robb, J. R. Cheeseman, G. Scalmani, V. Barone, B. Mennucci, G. A. Petersson, H. Nakatsuji, M. Caricato, X. Li, H. P. Hratchian, A. F. Izmaylov, J. Bloino, G. Zheng, J. L. Sonnenberg, M. Hada, M. Ehara, K. Toyota, R. Fukuda, J. Hasegawa, M. Ishida, T. Nakajima, Y. Honda, O. Kitao, H. Nakai, T. Vreven, Jr. J. A. Montgomery, J. E. Peralta, F. Ogliaro, M. Bearpark, J. J. Heyd, E. Brothers, K. N. Kudin, V. N. Staroverov, R. Kobayashi, J. Normand, K. Raghavachari, A. Rendell, J. C. Burant, S. S. Iyengar, J. Tomasi, M. Cossi, N. Rega, J. M. Millam, M. Klene, J. E. Knox, J. B. Cross, V. Bakken, C. Adamo, J. Jaramillo, R. Gomperts, R. E. Stratmann, O. Yazyev, A. J. Austin, R. Cammi, C. Pomelli, J. W. Ochterski, R. L. Martin, K. Morokuma, V. G. Zakrzewski, G. A. Voth, P. Salvador, J. J. Dannenberg, S. Dapprich, A. D. Daniels, O. Farkas, J. B. Foresman, J. V. Ortiz, J. Cioslowski, D. J. Fox, Gaussian 09 Revision A.02, Gaussian Inc., Wallingford CT, 2009.

[32] a) J. P. Perdew, K. Burke, M. Ernzerhof, *Phys. Rev. Lett.* **1996**, *77*, 3865-3868; b) C. Adamo, V. Barone, *J. Chem. Phys.* **1999**, *110*, 6158-6170.
[33] F. Weigend, R. Ahlrichs, *Phys. Chem. Chem. Phys.* **2005**, *7*, 3297-3305.
[34] J. Tomasi, B. Mennucci, R. Cammi, *Chem. Rev.* **2005**, *105*, 2999-3093.
[35] a) M. Cossi, V. Barone, *J. Chem. Phys.* **2001**, *115*, 4708-4717; b) R. Improta, V. Barone, G. Scalmani, M. J. Frisch, *J. Chem. Phys.* **2006**, *125*, 054103-054109.
[36] A.-R. Allouche, *J. Comput. Chem.* **2011**, *32*, 174-182.

Entry for the Table of Contents

Layout 1:

Lanthanides

Series of lanthanide compounds made from chiral Phenantroline-based Helicate Like Ligands displayed either magnetic or emissive properties.

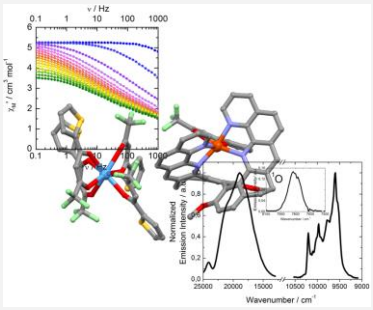

S. Speed, F. Pointillart,* J.-C. Mulatier, L. Guy,* S. Golhen, O. Cador, B. Le Guennic, F. Riobé, O. Maury, L. Ouahab Page No. – Page No.

Photophysical and Magnetic Properties in Complexes Associating 3d/4f Elements and Chiral Phenantroline-based Helicate Like Ligands

Keywords: Helicene, Lanthanides, Iron, chirality, luminescence, Magnetic Properties